

Vibrationally resolved charge transfer and ionisation cross sections for ion-H₂(D₂, DT, T₂) collisions

D. Elizaga, L.F. Errea, J.D. Gorfinkiel, C. Illescas, A. Macías¹,
L. Méndez, I. Rabadán, A. Riera, A. Rojas, P. Sanz

Departamento de Química, Universidad Autónoma de Madrid,
Madrid, Spain

Abstract. Theoretical (*ab initio* and CMTC) cross sections for charge transfer and ionization in ion-H₂ collisions are presented. Vibrationally resolved cross sections are obtained for some ions using the sudden and Franck-Condon approximations along with some vibrational close-coupling calculations. Our results are compared with experimental data and other theoretical results.

1. Introduction

Charge transfer cross sections in collisions of multicharged ions with molecules are of interest in the outer regions of the plasma in fusion devices, particularly near divertors. In this paper we summarize calculated cross sections for collisions of ions with H₂ (also D₂, DT and T₂) for energies above 40 eV/amu. Our methods are based on the sudden approximation for the treatment of the ro-vibrational motion of the diatom. In some cases, we have used the additional Franck-Condon (FC) approximation and the cross sections have been obtained from calculations at only the target equilibrium distance ρ_0 . Partial vibrational cross sections can be obtained in this case, by multiplying the FC ones by the FC factors of Table 1 [1]. At low velocities, we have employed a close-coupling expansion for the electronic wavefunction in terms of *ab initio* molecular functions (see [2]).

State-to-state vibrational cross sections have been calculated in collisions of Be⁴⁺ [3], C⁴⁺ [4], H⁺ and C²⁺(³P) [5] with H₂ in the impact energy range 50 eV/amu–2 keV/amu. Significant deviations from the simple FC approximation were found; hence, explicit comparison with vibrationally resolved measured data is useful.

In each case, the molecular states used in the dynamical study were chosen from consideration of the adiabatic correlation diagrams. The asymptotic energy differences between the electronic states and the corresponding experimental ones [6] are always smaller than 10^{−2} Hartree.

When the correlation diagram is too complex or at intermediate impact velocities, when a large number of molecular states are required in the dynamical treatment, a model potential approach has been applied.

At high impact energies (9–625 keV/amu for charge transfer and 9 keV/amu–2.5 MeV/amu for ionisation) classical trajectory calculations have been carried out [7].

Comparison with other experimental results and calculations (not shown in the figures) are included in the published papers mentioned in the corresponding sections.

¹ Also at Instituto de Estructura de la Materia CSIC, Serrano 113 bis, 28006 Madrid, Spain.

Cross sections are tabulated as a function of the relative impact velocity, v (in a.u.), and the corresponding energies are $E = 24.982 v^2$ keV/amu.

2. Theory

The method we use is described in detail in [3]. Here we only summarize the procedure:

1. Molecular data (energies and dynamical couplings) for the triatomic AH_2^q are obtained *ab initio* using MELD [2], modified as explained in [8].
2. The sudden approximation for rotation and vibration is employed to obtain the vibrational state-to-state cross sections. The electronic transitions are calculated using the semiclassical eikonal method (see e.g. [9]): for fixed H_2 target position, the ion follows rectilinear trajectories with impact parameter \mathbf{b} and velocity \mathbf{v} , $\mathbf{R} = \mathbf{b} + \mathbf{v}t$. The wavefunction Ψ describing the collision is solution of

$$\left(H_{\text{int}} - i \frac{\partial}{\partial t} \right) \Psi(\mathbf{r}, \boldsymbol{\rho}, t) = 0 \quad (1)$$

where $H_{\text{int}} = H_{\text{el}} + T_\rho$ is the total Hamiltonian without the kinetic energy term associated to the coordinate R . The wavefunction Ψ is expanded as:

$$\Psi(\mathbf{r}, \boldsymbol{\rho}, t) = \chi_0(\rho) Y_{JM}(\hat{\boldsymbol{\rho}}) \sum_k a_k(\boldsymbol{\rho}, t) \phi_k(\mathbf{r}; \mathbf{R}, \boldsymbol{\rho}) \exp \left(-i \int_0^t \epsilon_k dt' \right) \quad (2)$$

where $\chi_0(\rho) Y_{JM}(\hat{\boldsymbol{\rho}})$ is the initial rovibrational wavefunction of H_2 , and $\phi_k(\mathbf{r}; \mathbf{R}, \boldsymbol{\rho})$ are electronic wavefunctions of the triatomic quasimolecule with energies ϵ_k .

These functions ϕ_k depend on three parameters: R , the distance from the projectile to the H_2 centre of mass; ρ , the H-H internuclear distance; and θ , the angle between \mathbf{R} and $\boldsymbol{\rho}$.

2.1. Isotropic approximation

When charge transfer transitions occur at relatively large R , anisotropy effects in the projectile-target interactions are small and both the hamiltonian and the dynamical couplings may be substituted by those obtained for a fixed value of θ .

Substituting (2) in (1) leads to a set of differential equations for the coefficients a_k . The probability $P_{\nu f}$ for transition from the vibronic state $\{0i\}$ to $\{\nu f\}$ is given by

$$P_{\nu f}(b, v) = \left| \int d\rho \chi_0 \chi_\nu \exp \left[-i \int_0^\infty dt (\epsilon_f - E_f) \right] a_f(\infty, \rho) \right|^2 \quad (3)$$

where E_f is the asymptotic energy of the vibronic state $\{\nu f\}$. The total cross section for the transition $\{0i\} \rightarrow \{\nu f\}$ is, in the isotropic approximation [1],

$$\sigma_{\nu f}(v) = 2\pi \int_0^\infty b P_{\nu f} db. \quad (4)$$

It is useful to define the quantities $P_n^e(\rho, b, v)$ and $\sigma_n^e(\rho, v)$ for a fixed ρ and v as

$$P_f^e(\rho, b, v) = |a_f(\infty, \rho)|^2 \quad (5)$$

$$\sigma_f^e(\rho, v) = 2\pi \int_0^\infty b P_f^e(\rho, b, v) db. \quad (6)$$

When $\rho = \rho_0$, the target equilibrium distance, equations (5) and (6) yield the familiar FC transition probability and cross section respectively.

From equation (4), and using the closure relations for the vibrational functions χ_ν , the total cross section for transition to the electronic state f is given by

$$\sigma_f(v) = \sum_\nu \sigma_{\nu f} = \int_0^\infty \chi_0^2 \sigma_f^e d\rho. \quad (7)$$

2.2. Anisotropic behaviour

When transitions occur at small R distances, the isotropic approximation is not longer accurate and an average over the relative orientations must be performed. Then, the vibronic probabilities (equation (3)) and cross sections (equation (4)) become (see e.g. Errea et al. [3])

$$P_{\nu f}(\mathbf{v}, \hat{\boldsymbol{\rho}}) = \left| \int d\rho \chi_0 \chi_\nu \exp \left[-i \int_0^\infty dt (\epsilon_f - E_f) \right] a_f(\infty, \boldsymbol{\rho}) \right|^2 \quad (8)$$

and

$$\sigma_{\nu f}(v) = \frac{1}{4\pi} \int d\mathbf{b} \int d\hat{\boldsymbol{\rho}} P_{\nu f}(\mathbf{v}, \hat{\boldsymbol{\rho}}). \quad (9)$$

The presence of divergent rotational couplings at the conical intersections between adiabatic states was solved by removing the divergent components from the rotational couplings [10].

2.3. Model potential calculations

The *ab initio* calculation of charge transfer cross sections in collisions of multiply charged ions with H₂ molecules becomes cumbersome when a large number of coupled states has to be included in the basis. This is always the case at higher impact velocities.

An alternative approach, (see e.g. [9] and references therein), is the use of effective potentials to treat the interaction of the active electron, described by a model wavefunction $\psi^m(\mathbf{r}, t)$, with the cores.

Firstly, we solve the one-electron impact parameter model equation

$$\left(h^m - i \frac{\partial}{\partial t} \right) \psi^m(\mathbf{r}, t) = 0 \quad (10)$$

where h^m includes model potentials of the form:

$$V_k = -\frac{Z - N_c}{r_k} - \frac{N_c}{r_k} (1 + \alpha_k r_k) \exp(-\alpha'_k r_k) \quad (11)$$

to describe the interaction of the active electron with the X^{q+} projectile and H₂⁺ cores respectively. $\psi^m(\mathbf{r}, t)$ is expanded in terms of (approximate) MO χ_j , eigenfunctions of h^m with energies ϵ_j :

$$\psi^m(\mathbf{r}, t) = D(\mathbf{r}, t) \sum_j a_j(t) \chi_j \exp(-i \int_0^t \epsilon_j dt') \quad (12)$$

where $D(\mathbf{r}, t)$ is a common translation factor (CTF) [11–13].

Then, a two-electron interpretation is required to evaluate transition probabilities and cross sections. In the usual equivalent-electron independent particle model (IPM) approach, [14–16], the two-electron impact parameter equation:

$$\left[H - i \frac{\partial}{\partial t} \right] \Psi(\mathbf{r}_1, \mathbf{r}_2, t) = 0 \quad (13)$$

is simplified by replacing H by the IPM Hamiltonian H^{IPM}

$$H^{\text{IPM}} = h^m(1) + h^m(2) \quad (14)$$

and the solution of (13) is approximated by

$$\Psi^{\text{IPM}}(\mathbf{r}_1, \mathbf{r}_2, t) = ||\psi^m \overline{\psi^m}|| \quad (15)$$

where $|| \ ||$ denotes a Slater determinant.

The IPM transition probabilities for single electron capture (SEC) (P^{SEC}), double electron capture (DEC) (P^{DEC}) and excitation (EX) (P^{EX}) are obtained by projecting Ψ^{IPM} onto the corresponding asymptotic forms of the electronic states in the limit $t \rightarrow \infty$. This method has been previously applied to ion- H_2 collisions in ref. [7]. However, this standard IPM interpretation, leads to inaccurate results at low velocities. For example, P^{SEC} is always less than 0.5 which points to a limitation of the IPM.

2.3.1. IPM-SEC approximation

To improve the IPM in the treatment of SEC at low velocities, we have applied a modified technique, the IPM-SEC method. We construct a set of diabatic MOs $\{\chi_j^d\}$ [17], by a unitary transformation of the set $\{\chi_j\}$. We then construct the set of two-electron wavefunctions $\phi_{kl}(\mathbf{r}_1, \mathbf{r}_2, t)$:

$$\phi_{kl} = \frac{N_{kl}}{\sqrt{2}} \left[||\chi_k^d \bar{\chi}_l^d|| + ||\chi_l^d \bar{\chi}_k^d|| \right] \quad (16)$$

where $N_{kl} = 2^{-1/2}$ for $k = l$ and $N_{kl} = 1$ for $k \neq l$. The IPM-SEC wavefunction $\Psi^{\text{IPM-SEC}}$ is then expanded as:

$$\Psi^{\text{IPM-SEC}} = D(\mathbf{r}_1, \mathbf{r}_2, t) \sum_{kl} a_{kl}(t) \phi_{kl}(\mathbf{r}_1, \mathbf{r}_2) \exp[-i \int_0^t E_{kl} dt'] \quad (17)$$

with $E_{kl} = \langle \phi_{kl} | H | \phi_{kl} \rangle$.

For systems where the interactions between both the entrance channel and SEC functions with DEC functions are not effective, these DEC functions can be removed from expansion (17).

As in the standard IPM approach, [18], the matrix elements of H can be replaced by those of H^{IPM} of eq. (14). Time integration of the ensuing system of differential equations then yields the expansion coefficients a_{jk} , and hence the SEC and excitation transition probabilities.

3. Results

3.1. $\text{H}^+ + \text{H}_2(\text{X}^1 \Sigma_g^+, \nu)$

We have obtained single electron capture (SEC) vibrationally resolved cross section using the sudden approximation. The basis set includes the lowest two states of H_3^+ . SEC cross sections from $\nu=0$ and $\nu=1$ of $\text{H}_2(\text{X}^1 \Sigma_g^+)$ are given in Table 2 and plotted in Figure 1. Also plotted in this figure are the capture to dissociative vibrational states (DC), total vibrational excitation (VE) and dissociative excitation (DE) cross sections.

Comparison with experimental data for capture of Gealy and van Zyl [19] shows a good agreement at impact velocities above 0.1 a.u., while a sizeable difference may be observed at lower values with Sudden calculations. To ascertain the origin of this discrepancy, we have carried out a vibronic close-coupling calculation (CC) using 7 states corresponding to the entrance $\text{H}^+ + \text{H}_2$ channel and other 7 states corresponding to the capture $\text{H}(1s) + \text{H}_2^+$ state. The excellent agreement obtained with experimental measurements shows the region of validity of the Sudden approach.

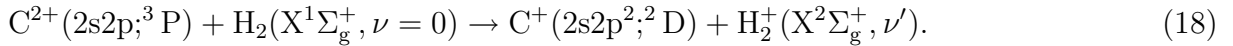
State-to-state vibrational cross sections are shown in figures 2 (capture) and 3 (excitation), (see also [1]), for H_2 , D_2 , DT , and T_2 targets.

3.2. $\text{Li}^+ + \text{H}_2$

A 5-electronic-state calculation for the system LiH_2^+ was performed [1] in the framework of the FC approximation. Orientation averaged cross sections (eq. 8-9) for SEC to $\text{Li}(2s, 2l) + \text{H}_2^+$ and excitation to $\text{H}_2(\text{B } ^1\Sigma_u^+)$ are given in Table 3 and plotted in Figure 4.

3.3. $\text{C}^{2+} + \text{H}_2$

13- and 16- state calculations were performed for the ground ($2s^2; ^1\text{S}$) and metastable ($2s2p; ^3\text{P}$) states of C^{2+} respectively. The collinear geometry and the FC approximation were employed [20]. Results are shown in Figure 5 and Table 4. More accurate calculations, using the sudden approximation, have been also carried out for collisions with the metastable projectile [5]. In this case, cross sections to individual vibrational states of H_2^+ have been obtained in the process:



and compared to measured distributions [21], obtained after increased the resolution of the experiment.

We also include in figure 5 the more accurate sudden total cross section $\sigma_{2\text{D}}$ calculated using (7) from $\text{C}^{2+}(^3\text{P})$. Good agreement between this and the FC approximation is found for high energies, but differences are noticeable at the low impact energies.

In figure 6, we show the vibrational distributions of $\text{H}_2^+(\text{X}^2\Sigma_g^+, \nu')$ for reaction (18) at four impact energies. As in [21], in the range of impact energies (0.6–1 keV), our *sudden* distributions show a maximum at $\nu' = 4$, which moves to smaller ν' as the impact energy increases, approaching the FC prediction.

This behaviour can be explained by expanding $a_f(\rho)$ in powers of $(\rho - \rho_c)$ in equation (3) and (4). Corrected FC cross sections are obtained as explained in [5], and plotted in figure 6, where they display a better agreement with the more exact results.

The calculated state-to-state charge transfer cross sections are compared to the experimental TES of [21] at $E = 1$ keV in figure 7.

Very good agreement is obtained for the vibrational distribution of H_2^+ associated with the $\text{C}^+(^2\text{D})$ ions, which confirms the accuracy of the vibrational sudden approximation method for this energy range and of the experimental data. The small values obtained for the $\text{C}^+(^2\text{S})$ band, do not allow to get any conclusion when compared to the experimental values.

3.4. $\text{C}^{3+} + \text{H}_2$

Calculations have been carried out using the FC approximation, collinear geometry and a basis of 8 electronic states. DEC leading to Coulomb explosion of the diatom is competitive with SEC and the corresponding cross sections are listed in Table 5 and plotted in Figure 8.

3.5. $\text{C}^{4+} + \text{H}_2$

Calculations using the sudden approximation and a basis of 8 electronic states were reported in [4]. Our results include state-selected (vibrational and electronic) cross sections in SEC, as well as cross sections for transfer dissociation and vibrational excitation in collisions with H_2 , D_2 and DT . We give cross sections for SEC into the main exit electronic channels in Table 6 and Figure 9.

IPM-SEC treatment

To extend the energy range, to $50 \text{ eV/amu} \leq E \leq 6 \text{ keV/amu}$, we have employed the IPM-SEC model approach. The interaction with the H_2^+ core (see [18]) is described by a one-center model potential (eq. (11)). Details on the model potential parameters are described in [18]. A semiclassical impact parameter treatment, in the framework of the Franck-Condon approximation calculation is carried out, whose accuracy for total and partial SEC cross sections was discussed in ref. [4]. Our basis set includes 20 MOs and the CTF of ref. [12].

In figure 10 we have included the IPM-SEC cross section.

3.6. $\text{N}^{5+} + \text{H}_2$

A model potential IPM-SEC treatment has been used in the FC framework. In this case, a more sophisticated two-center model potential (of (11)) has been used, to improve the representation of the H_2 target, as anisotropy effects are expected to be important. The basis set included 8 MOs: five dissociating into $\text{N}^{4+}(n=3)+\text{H}_2^+$, the two most important molecular orbital dissociating into $\text{N}^{4+}(n=4)+\text{H}_2^+$ and the entrance channel. Our results are given in Table 7 and plotted in Figure 11 together with experimental data of [22].

Although comparison with experimental data shows an overall agreement for the total single capture cross section to $N^{4+}(n=3)+H_2^+$, further calculations using *ab initio* data and the Sudden approach should be performed at lower velocities, as for this system, the double capture transitions to $N^{3+}(3l3l')$ compete with single capture.

3.7. CTMC calculations

We have calculated SEC and single ionisation (SI) cross sections for H^+ , He^{2+} , Li^{3+} , Be^{4+} , B^{5+} , C^{6+} , N^{7+} and O^{8+} in collisions with H_2 , using the improved impact parameter CTMC treatment (see [7]). The calculation employs the FC approximation and a model potential for the H_2 target. Results for SI are plotted in Figure 12 and tabulated in Table 8. The corresponding SEC results are given in Figure 13 and Table 9. In these figures, the results are compared with experimental and other theoretical data (see [7] for details).

Analogously to the ion-atom case, we have obtained scaling laws of the SEC and SI cross sections as functions of the charge q of the projectile and velocity v .

$$\sigma_{SEC}^{scaled}(q, vq^{0.11}) = \sigma_{SEC}(1, v)q \quad (19)$$

$$\sigma_{SI}^{scaled}(q, v) = \sigma_{SI}(1, v)q^2 \{0.92 - \exp[-0.57(v-0.01q)] - \exp[-1.8(v^2-0.08q)]\} \quad (20)$$

4. Concluding remarks

In the last few years, we have developed new methods to treat ion- H_2 collisions with a similar accuracy to those of ion-atom. These methods have been applied to several ions. We plan to extend our calculations to lower velocities of interest in cold regions of fusion plasma. A more detailed treatment of the anisotropy in the ion-target interaction has also been considered for when transitions occur at small distances. Calculations involving projectiles in both ground and metastable states are being carried out where experimental uncertainties in the composition of the initial beams exist.

ACKNOWLEDGEMENTS

This research has been partially supported by the DGICYT Project PB96-0056. IR acknowledges MEC for a Contrato de Incorporación de doctores. CI acknowledges MEC for a postdoctoral grant under the program SGPDE.

REFERENCES

- [1] D. ELIZAGA, L.F. ERREA, J.D. GORFINKIEL, A. MACÍAS, L. MÉNDEZ, A. RIERA, A. ROJAS, *J. Phys. B: At. Mol. Opt. Phys.*, 33:2037, 2000.
- [2] DAVIDSON. In E. CLEMENTI, editor, *MOTEC, Modern Techniques in Computational Chemistry*. ESCOM Publishers B. V., Leiden, 1990.
- [3] L.F. ERREA, J.D. GORFINKIEL, A. MACÍAS, L. MÉNDEZ, A. RIERA, *J. Phys. B: At. Mol. Opt. Phys.*, 30:3855, 1997.
- [4] L.F. ERREA, J.D. GORFINKIEL, A. MACÍAS, L. MÉNDEZ, A. RIERA, *J. Phys. B: At. Mol. Opt. Phys.*, 32:1705, 1999.
- [5] L.F. ERREA, A. MACÍAS, L. MÉNDEZ, I. RABADÁN, A. RIERA, *J. Phys. B: At. Mol. Opt. Phys.*, 33:L615, 2000.
- [6] C.E. MOORE, *Atomic Energy Levels, Nat. Stand. Ref. Data Series vol 1*. (US National Bureau of Standards), 1972.
- [7] C. ILLESCAS, A. RIERA, *Phys. Rev. A*, A60:4546, 1999.
- [8] J.F. CASTILLO, L.F. ERREA, A. MACÍAS, L. MÉNDEZ, A. RIERA, *J. Chem. Phys.*, 103:2113, 1995.
- [9] B.H. BRANSDEN, M.H.C. McDOWELL, *Charge Exchange and the Theory of Ion-Atom Collisions*. (Oxford: Clarendon), 1992.
- [10] D. ELIZAGA, L.F. ERREA, A. MACÍAS, L. MÉNDEZ, A. RIERA, A. ROJAS, *J. Phys. B: At. Mol. Opt. Phys.*, 32:L697, 1999.
- [11] S.B. SCHNEIDERMAN, A. RUSSEK, *Phys. Rev.*, 181:311, 1969.
- [12] C. HAREL, H. JOUIN, *J. Phys. B: At. Mol. Opt. Phys.*, 25:221, 1992.
- [13] L.F. ERREA, L. MÉNDEZ, A. RIERA, *J. Phys. B: At. Mol. Opt. Phys.*, 15:101, 1982.
- [14] J.H. McGUIRE, L. WEAVER, *Phys. Rev. A*, 16:41, 1977.
- [15] V.A. SIDOROVICH, *J. Phys. B: At. Mol. Phys.*, 14:4805, 1981.
- [16] H.J. LÜDDE, R.M. DREIZLER, *J. Phys. B: At. Mol. Phys.*, 16:3973, 1983.
- [17] F.T. SMITH, *Phys. Rev.*, 179:111, 1969.
- [18] L.F. ERREA, J.D. GORFINKIEL, C. HAREL, H. JOUIN, A. MACÍAS, L. MÉNDEZ, B. PONS, A. RIERA, *J. Phys. B: At. Mol. Opt. Phys.*, 33:3107, 2000.
- [19] M.W. GEALY, B.I. VAN ZYL, *Phys. Rev. A*, 36:3091, 1987.
- [20] L.F. ERREA, A. MACÍAS, L. MÉNDEZ, A. RIERA, *J. Phys. B: At. Mol. Opt. Phys.*, 32:4065, 1999.
- [21] P. LEPUTSCH, D. DUMITRIU, F. AUMAYR, H.P. WINTER, *J. Phys. B: At. Mol. Opt. Phys.*, 30:5009, 1997.
- [22] G. LUBINSKI, Z. JUHÁSZ, R. MORGENSTERN, R. HOEKSTRA, *Phys. Rev. Lett.*, 86:616, 2001.
- [23] G.W. McCLURE, *Phys. Rev.*, 1480:47, 1966.
- [24] M. KIMURA, *Phys. Rev. A*, 32:802, 1985.
- [25] F. AUMAYR, H.P. WINTER, *At. Data Nucl. Data Tables*, 65:155, 1985.
- [26] J. VanECK, J. KISTEMAKER, *Physica*, 26:629, 1960.
- [27] E. UNTERREITER, J. SCHWEINZER, H.P. WINTER, *J. Phys. B: At. Mol. Opt. Phys.*, 24:1003, 1991.
- [28] A. ITOH, *J. Phys. Soc. Jap.*, 64:3255, 1995.
- [29] K. OKUNO, *Tokyo Metropolitan University Report*, 2000.
- [30] J.B. GREENWOOD, *Private communication*.

- [31] R. HOEKSTRA, J.P.M. BEIJERS, A.R. SCHALATMANN, R. MORGENSTERN, F.J. DE HEER, *Phys. Rev. A*, 41:4800, 1990.
- [32] A. PHANEUF, I. ALVAREZ, F.W. MEYER, D.H. CRANDALL, *Phys. Rev. A*, 26:1892, 1982.
- [33] D. DIJKKAMP, D. CIRIC, E. VLIEG, A. DE BOER, J. DE HEER, *J. Phys. B: At. Mol. Opt. Phys.*, 18:4763, 1985.
- [34] M. GARGAUD, R. McCARROLL, *J. Phys. B: At. Mol. Phys.*, 18:463, 1985.
- [35] M. GARGAUD, PhD thesis, Université de Bordeaux I, 1987.
- [36] A. KUMAR, B. SAHA, *Phys. Rev. A*, 59:1273, 1999.
- [37] W. FRITSCH, *Phys. Rev. A*, 46:3910, 1992.

TABLE 1. FRANCK-CONDON FACTORS FOR H₂, D₂, DT AND T₂

ν'	H ₂	D ₂	DT	T ₂
0	0.088088	0.032798	0.023775	0.015375
1	0.163359	0.086461	0.068723	0.049741
2	0.181715	0.129654	0.111744	0.089406
3	0.159648	0.146563	0.135583	0.118563
4	0.123301	0.139736	0.137472	0.130021
5	0.088460	0.119268	0.123728	0.125349
6	0.060893	0.094501	0.102574	0.110319
7	0.041047	0.071197	0.080280	0.090900
8	0.027458	0.051864	0.060352	0.071390
9	0.018389	0.036974	0.044134	0.054148
10	0.012398	0.026026	0.031692	0.040062
11	0.008440	0.018211	0.022508	0.029137
12	0.005807	0.012731	0.015899	0.020957
13	0.004033	0.008925	0.011218	0.014979
14	0.002816	0.006293	0.007932	0.010679
15	0.001961	0.004470	0.005635	0.007618
16	0.001342	0.003204	0.004030	0.005450
17	0.000873	0.002318	0.002905	0.003919
18		0.001693	0.002112	0.002835
19		0.001247	0.001550	0.002067
20		0.000925	0.001147	0.001519
21		0.000689	0.000857	0.001125
22		0.000513	0.000644	0.000841
23		0.000378	0.000486	0.000634
24		0.000273	0.000368	0.000481
25		0.000189	0.000277	0.000368
26			0.000206	0.000282
27			0.000148	0.000217
28				0.000167
29				0.000127

TABLE 2. CROSS SECTIONS (IN UNITS OF 10^{-16} cm^2) FOR THE REACTIONS $\text{H}^+ + \text{H}_2(X^1\Sigma_g^+, \nu = 0, 1) \longrightarrow \text{H} + \text{H}_2^+(X^2\Sigma_g^+)$

$v(\text{a.u.})$	$\nu=0$	$\nu=1$	C.C
0.040			0.20
0.045	0.02	0.19	
0.063	0.11	0.64	0.43
0.089	0.45	1.68	0.65
0.100	0.69	2.20	0.78
0.141	2.07	4.47	1.68
0.200	4.79	7.00	4.34
0.400	8.99	9.15	

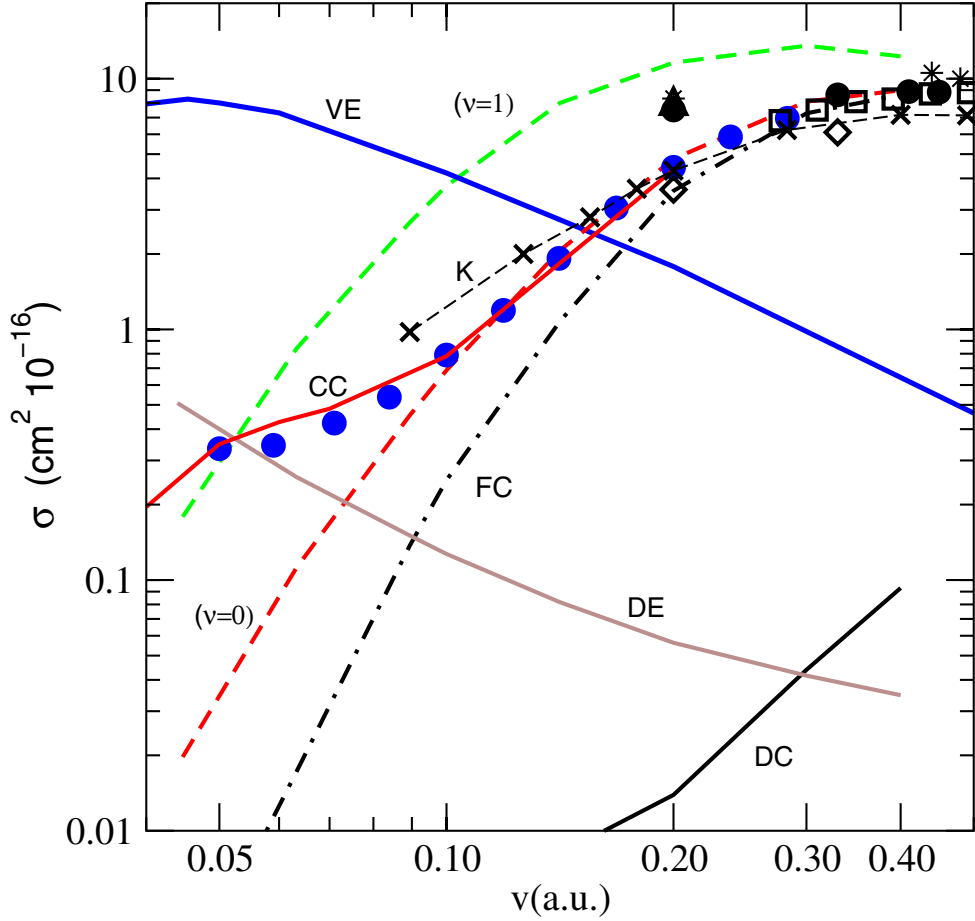


FIG. 1. Cross sections for the reactions $\text{H}^+ + \text{H}_2(X^1\Sigma_g^+; \nu) \longrightarrow \text{H} + \text{H}_2^+(X^2\Sigma_g^+)$. (●) Geally [19], (□) [23], (K) [24]; our results: (VE) vibrational excitation, (CC) vibrational close-coupling, (FC) Franck-Condon, (DE) dissociative excitations, (DC) dissociative capture, ($\nu = 0$) capture from $\text{H}_2(\nu = 0)$, ($\nu = 1$) capture from $\text{H}_2(\nu = 1)$. For other experimental data see ref. [1].

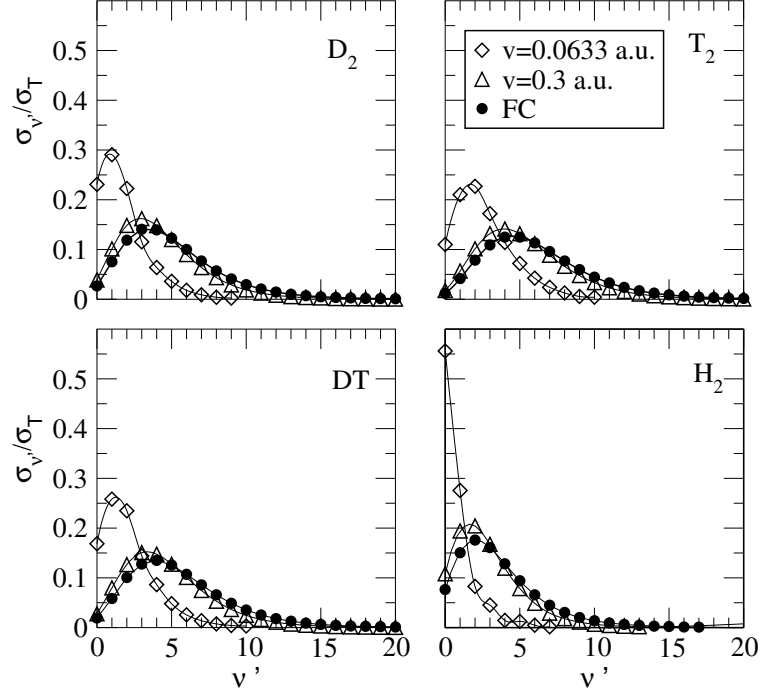


FIG. 2. Cross sections for the reactions $H^+ + H_2(X^1\Sigma_g^+; \nu) \rightarrow H + H_2^+(X^2\Sigma_g^+; \nu')$. Empty symbols are from the vibronic CC calculation (see text).

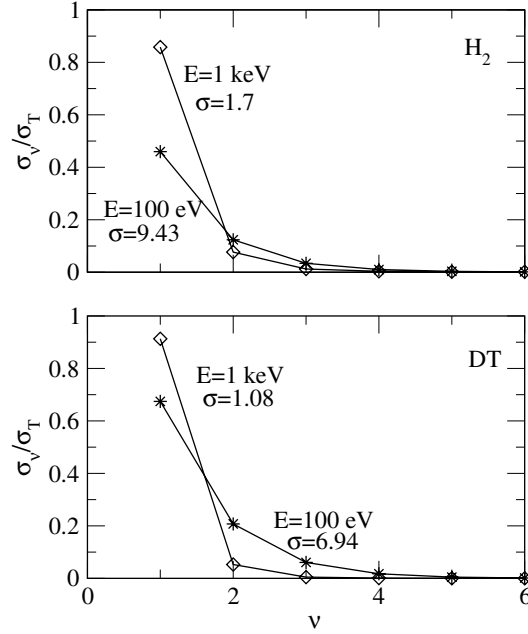


FIG. 3. Cross sections for the reactions $H^+ + H_2(X^1\Sigma_g^+; \nu=0) \rightarrow H^+ + H_2(X^1\Sigma_g^+; \nu)$.

TABLE 3. CROSS SECTIONS (IN UNITS OF 10^{-16} cm^2) FOR THE SEC REACTIONS $\text{Li}^+ + \text{H}_2 \rightarrow \text{Li}(2s) + \text{H}_2^+$ AND $\text{Li}^+ + \text{H}_2 \rightarrow \text{Li}(2l) + \text{H}_2^+$, AND THE EXCITATION REACTION $\text{Li}^+ + \text{H}_2(X \ ^1\Sigma_g^+) \rightarrow \text{Li}^+ + \text{H}_2(B \ ^1\Sigma_u^+)$

$v(\text{a.u.})$	$\text{Li}(2s)$	$\text{Li}(2l)$	$\text{H}_2(B \ ^1\Sigma_u^+)$
0.063	0.02	0.03	0.04
0.089	0.04	0.10	0.05
0.100	0.07	0.13	0.06
0.141	0.06	0.21	0.06
0.200	0.18	0.48	0.15
0.250	0.29	0.53	0.23
0.300	0.31	0.63	0.27
0.350	0.31	0.79	0.30
0.400	0.41	0.99	0.29
0.500	0.74	1.46	0.23

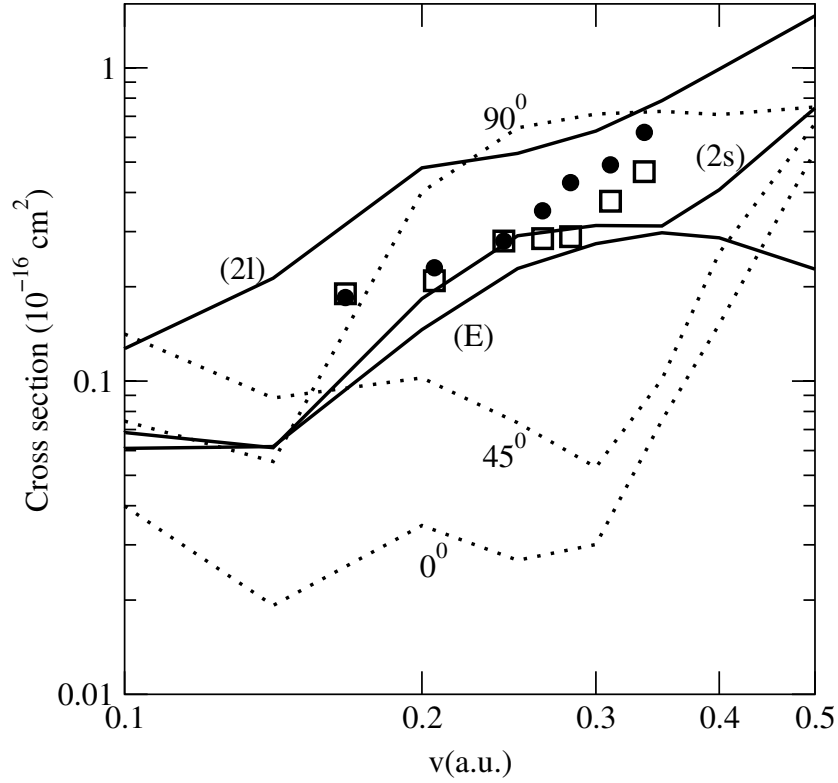


FIG. 4. Cross sections for the SEC reactions (2s) $\text{Li}^+ + \text{H}_2 \rightarrow \text{Li}(2s) + \text{H}_2^+$ and (2l) $\text{Li}^+ + \text{H}_2 \rightarrow \text{Li}(2l) + \text{H}_2^+$, and the excitation reaction (E) $\text{Li}^+ + \text{H}_2(X \ ^1\Sigma_g^+) \rightarrow \text{Li}^+ + \text{H}_2(B \ ^1\Sigma_u^+)$. Also plotted are the isotropic calculation (dotted lines) obtained for three values of the relative orientation angle α for capture to $\text{Li}(2s)$. \bullet [25], \square [26].

TABLE 4. FC SEC CROSS SECTIONS (IN UNITS OF 10^{-16} cm^2) FOR $\text{C}^{2+} + \text{H}_2(\text{X } ^1\Sigma_g^+)$ COLLISIONS

v (a.u.)	$\text{C}^{2+}(^1\text{S})(\text{FC})$	$\text{C}^{2+}(^3\text{P})(\text{FC})$	$\text{C}^{2+}(^3\text{P})(\text{sudden})$
0.045	6.053	17.606	12.425
0.048	5.808	17.919	12.799
0.052	5.490	17.975	12.803
0.055	5.309	18.440	13.138
0.058	5.140	18.587	13.509
0.060	5.102	18.484	13.650
0.080	5.460	19.219	15.098
0.100	6.143	18.836	15.378
0.115	6.763	17.162	14.646
0.120	6.828	16.475	14.282
0.140	7.379	14.656	13.148
0.160	8.165	14.132	12.546
0.180	8.952	13.738	12.024
0.200	9.302	13.118	11.418
0.220	9.587	12.352	10.753
0.240	9.873	11.556	10.079
0.260	10.130	10.801	9.432

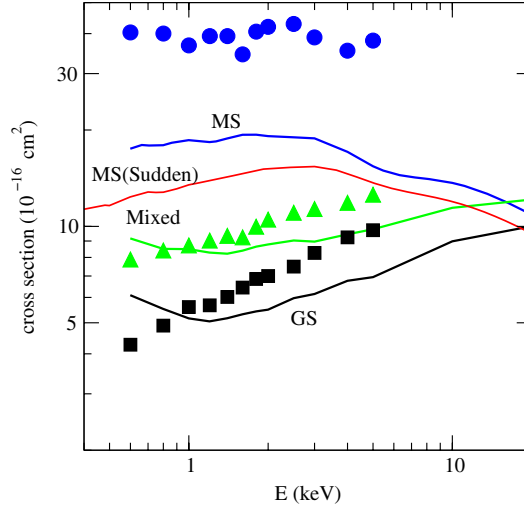


FIG. 5. Franck-Condon charge transfer cross section in the collision (GS) $\text{C}^{2+}(^2\text{S}) + \text{H}_2 \rightarrow \text{C}^+(^2\text{D}) + \text{H}_2^+$ and (MS) $\text{C}^{2+}(^3\text{P}) + \text{H}_2 \rightarrow \text{C}^+(^2\text{D}) + \text{H}_2^+$. Also included is the sudden cross section with projectile $\text{C}^{2+}(^3\text{P})$ (eq. (7)). Symbols are experiments of [27].

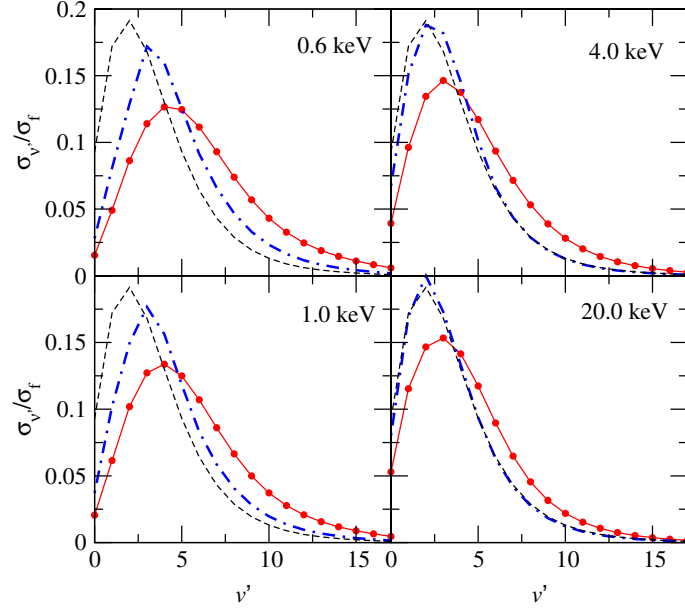


FIG. 6. Relative cross section $\sigma_{\nu'}/\sigma_f$ for the charge transfer reaction (18) as a function of $H_2^+(X^2\Sigma_g^+)$ vibrational state (ν'). Dotted continuous line are the sudden approximation results (equation 4). The dot-dashed line are the corrected FC results of equation (9) of [5] and the dashed line the FC results.

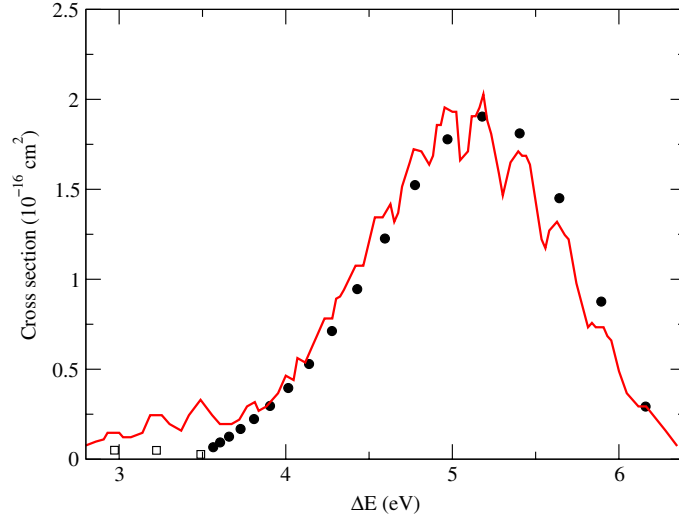


FIG. 7. Calculated cross section for the charge transfer reactions $C^{2+}(^3P) + H_2(X^1\Sigma_g^+, \nu = 0) \rightarrow C^+(^2D) + H_2^+(X^2\Sigma_g^+, \nu')$ (\bullet) and $C^{2+}(^3P) + H_2(X^1\Sigma_g^+, \nu = 0) \rightarrow C^+(^2S) + H_2^+(X^2\Sigma_g^+, \nu')$ (\square) at $E = 1$ keV as a function of energy defect. The curve corresponds to [21] experiment, renormalized to the area under the theoretical data.

TABLE 5. FC SEC AND DEC CROSS SECTIONS (IN UNITS OF 10^{-16} cm^2) FOR $\text{C}^{3+} + \text{H}_2$ COLLISIONS

$v(\text{a.u.})$	SEC	DEC
0.100	7.781	4.518
0.120	6.280	4.832
0.150	5.947	4.785
0.200	6.358	4.407
0.250	6.444	3.972
0.300	6.366	3.694
0.350	6.189	3.548
0.400	5.965	3.470
0.450	5.730	3.423
0.500	5.505	3.391

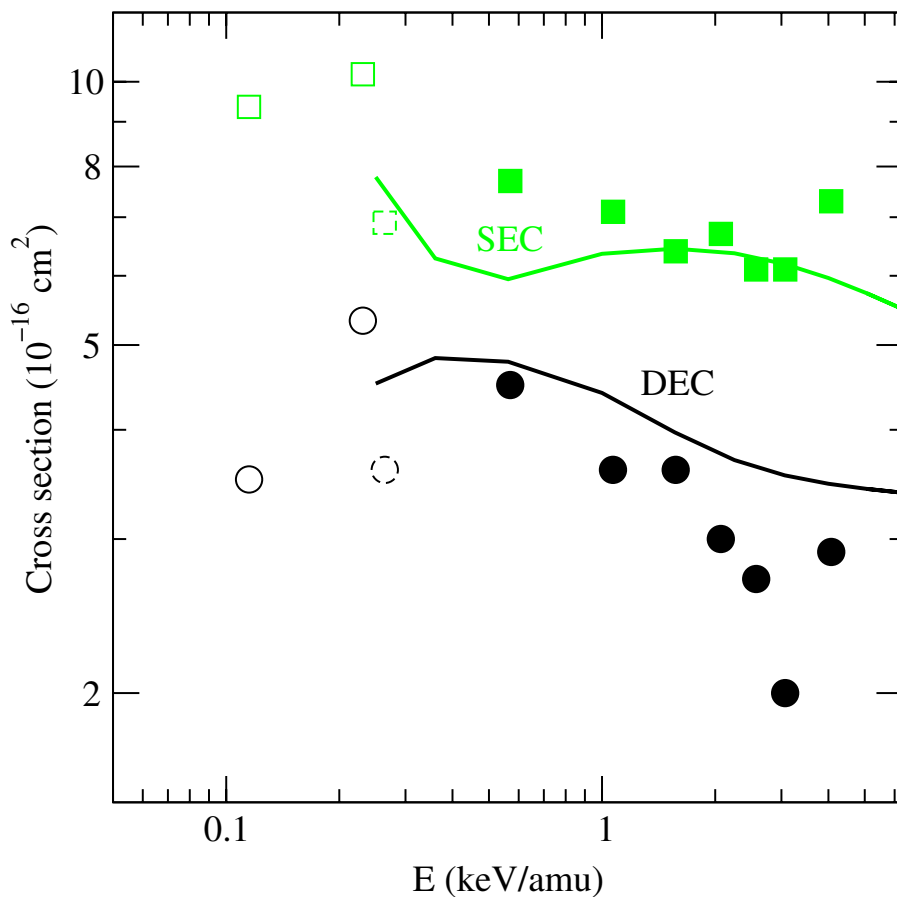


FIG. 8. FC SEC (light grey line and symbols) and DEC (black line and symbols) cross sections for the collision $\text{C}^{3+} + \text{H}_2$. Lines are our results. Full symbols: ref. [28]; empty symbols [29]; dashed line symbols [30].

TABLE 6. SUDDEN CROSS SECTIONS (IN UNITS OF 10^{-16} cm^2) FOR THE REACTION $\text{C}^{4+} + \text{H}_2 \rightarrow \text{C}^{3+}(1s^2 3l) + \text{H}_2^+(X^2\Sigma_g^+)$

$v(\text{a.u.})$	$l=0$	$l=1$	$l=2$	Total
0.045	16.9	24.7	1.1	42.8
0.060	20.1	20.7	1.1	42.0
0.071	21.4	18.4	1.2	40.9
0.077	21.8	17.7	1.3	40.8
0.089	22.1	17.3	1.7	41.1
0.100	22.1	16.9	2.2	41.3
0.122	22.2	14.9	3.0	40.0
0.141	22.1	12.4	3.7	38.1
0.200	19.9	9.6	3.8	33.3
0.253	17.1	9.8	3.9	30.8
0.300	14.9	9.7	4.4	29.1

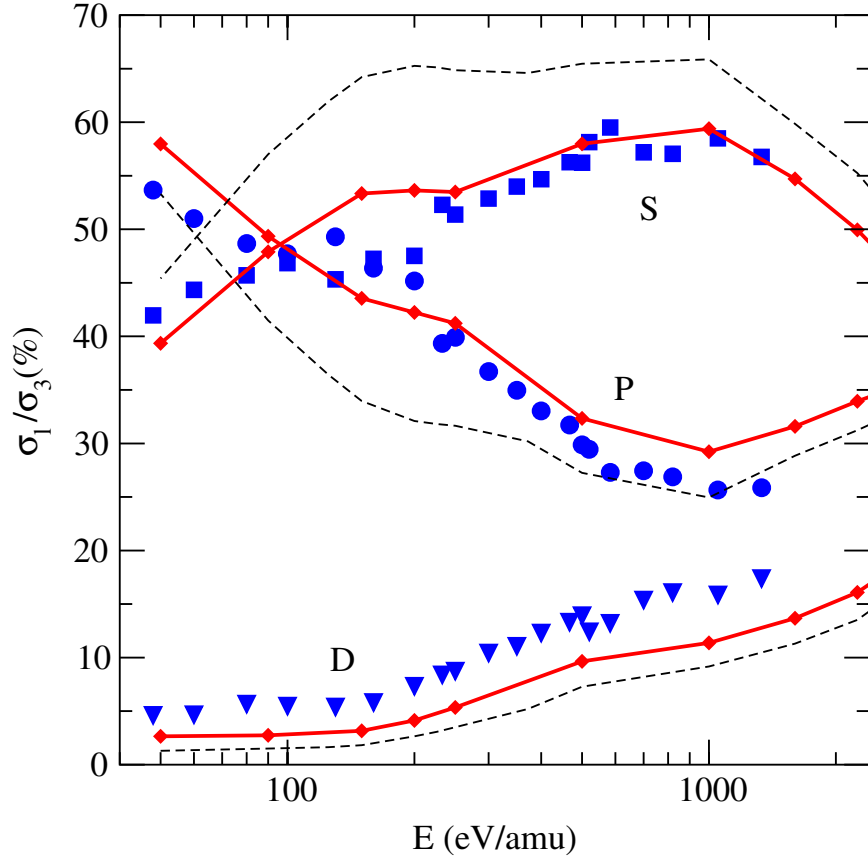


FIG. 9. Cross section fractions σ_l/σ_3 for the reaction $\text{C}^{4+} + \text{H}_2 \rightarrow \text{C}^{3+}(1s^2 3l) + \text{H}_2^+(X^2\Sigma_g^+)$. Solid line: Sudden approximation; dashed line: FC approximation [4]; symbols: experimental results [31].

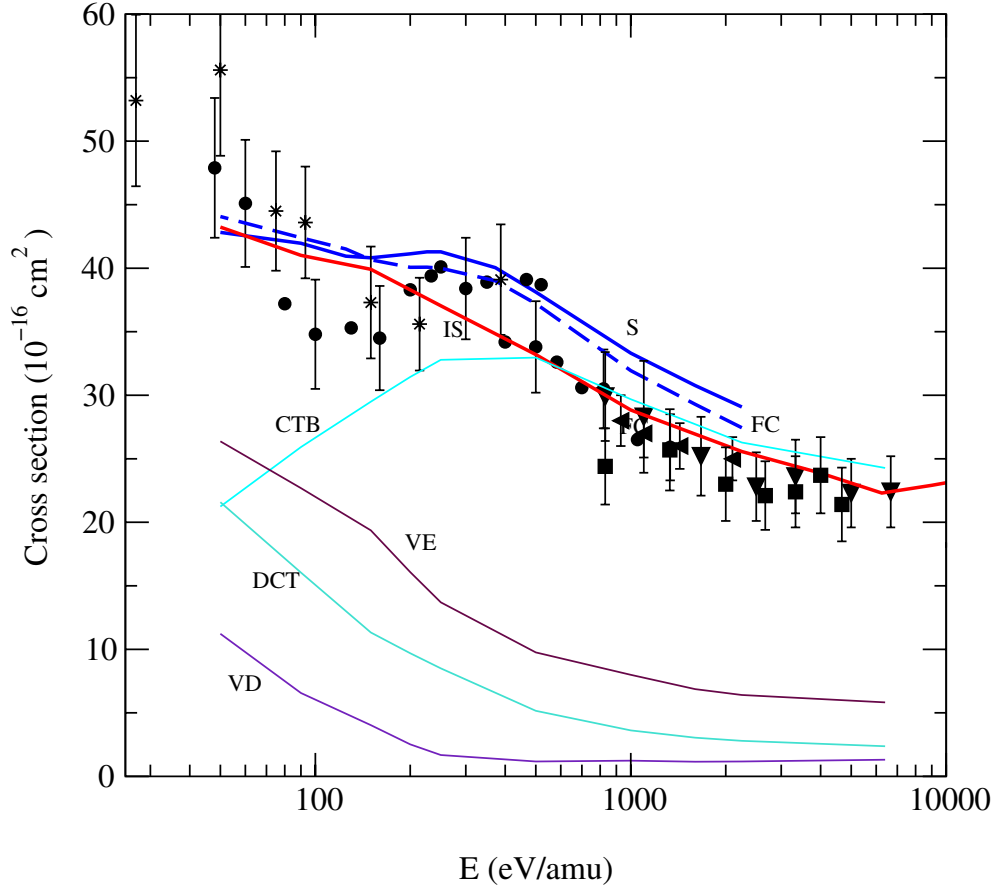


FIG. 10. Sudden cross sections for the reaction $C^{4+} + H_2 \rightarrow C^{3+}(1s^2 3l) + H_2^+(X \ ^2\Sigma_g^+)$. Our work: [4]; experimental: [32, 33, 28, 31] and previous effective potential calculations refs. [34–37]. (S) Sudden app.; (FC) Franck-Condon app.; (IS) IMP-SEC; (CTB) charge transfer to bound states; (VE) vibrational excitation; (DCT) dissociative charge transfer; (VD) vibrational dissociation.

TABLE 7. IPM-SEC TOTAL CHARGE TRANSFER CROSS SECTIONS (IN UNITS OF 10^{-16} cm^2) FOR THE COLLISION $\text{N}^{5+} + \text{H}_2$

$v(\text{a.u.})$	σ	$v(\text{a.u.})$	σ
0.0447	1.350	0.320	14.308
0.0632	2.271	0.330	14.819
0.089	3.752	0.340	15.453
0.100	4.250	0.350	16.155
0.125	5.427	0.360	16.864
0.150	6.486	0.370	17.532
0.175	7.623	0.380	18.131
0.200	9.236	0.390	18.662
0.210	9.861	0.400	19.095
0.220	10.380	0.410	19.397
0.230	10.743	0.425	19.610
0.240	11.162	0.440	19.565
0.250	11.680	0.450	19.469
0.260	12.200	0.460	19.370
0.270	12.649	0.500	19.428
0.300	13.656	0.540	20.238
0.310	13.938		

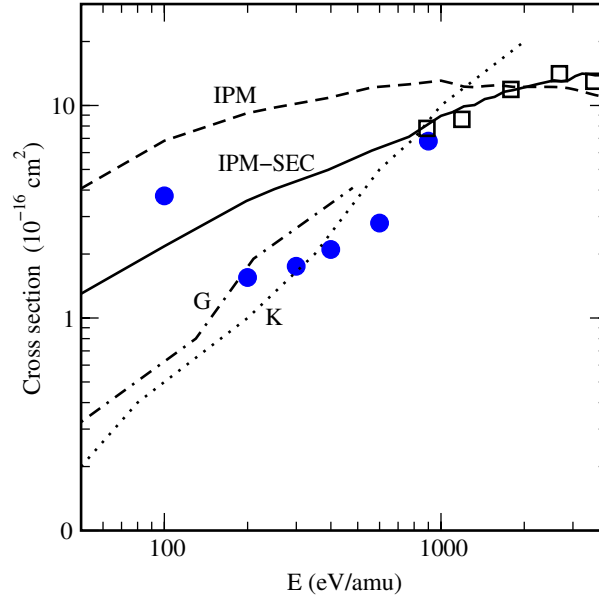


FIG. 11. Cross sections for population of $\text{N}^{4+}(1s^2 3l)$ in $\text{N}^{5+} + \text{H}_2$ collisions. Our results: lines labelled IPM and IPM-SEC; (G) [34], (K) [36], (\square) Exp. [33], (\bullet) Exp. [22].

TABLE 8. CMTC SINGLE IONIZATION CROSS SECTIONS (IN UNITS OF 10^{-16} cm^2) FOR $A^{q+} + \text{H}_2$ COLLISIONS, AS FUNCTIONS OF THE RELATIVE VELOCITY

$v(\text{a.u.})$	H^+	He^{2+}	Li^{3+}	Be^{4+}	B^{5+}	C^{6+}	N^{7+}	O^{8+}
0.6	0.235	0.112		0.019				
0.8	0.697	0.405	0.279	0.237	0.164	0.138		
1.0	1.095	1.023	0.877	0.814	0.773	0.684	0.642	0.538
2.0	2.069	5.511	9.036	12.502	15.724	18.893	21.735	24.304
3.0	1.232	3.732	6.549	9.741	13.191	16.697	20.511	24.295
5.0	0.301	1.615	3.119	4.786	6.677	8.750	10.978	13.410
8.0	0.199	0.725	1.486	2.413	3.454	4.613	5.8485	7.163
10.0	0.127	0.488	1.040	1.699	2.475	3.354	4.293	5.282
12.0	0.096	0.368	0.772	1.289	1.874	2.514	3.241	4.044
14.0	0.070	0.292	0.615	1.019	1.487	2.018	2.569	3.212
16.0	0.058	0.214	0.491	0.814	1.195	1.626	2.115	2.615

TABLE 9. CMTC SEC CROSS SECTIONS (IN UNITS OF 10^{-16} cm^2) FOR $A^{q+} + \text{H}_2$ COLLISIONS, AS FUNCTIONS OF THE RELATIVE VELOCITY

$v(\text{a.u.})$	H^+	He^{2+}	Li^{3+}	Be^{4+}	B^{5+}	C^{6+}	N^{7+}	O^{8+}
0.6	6.451	13.214						
0.8	5.932	12.286	18.396	22.872	29.422	34.684	39.955	45.012
1.0	4.608	10.557	16.251	21.724	27.234	32.679	38.133	43.432
2.0	0.237	0.799	1.491	2.503	3.812	5.210	6.937	8.910
3.0	0.018	0.063	0.133	0.184	0.253	0.341	0.444	0.563
5.0		0.002	0.004	0.004	0.004	0.004	0.005	0.007

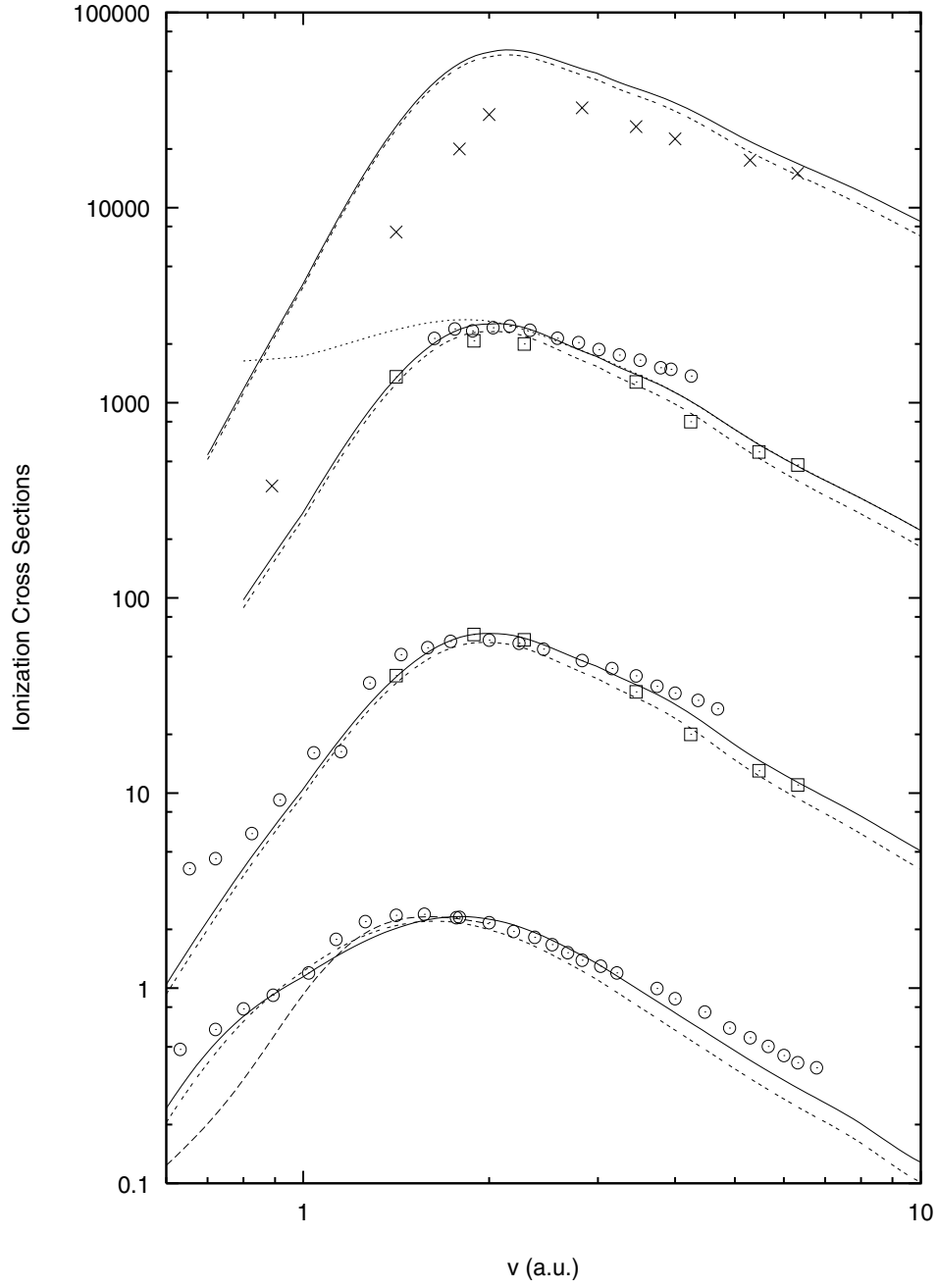


FIG. 12. SI cross sections as functions of the relative velocity v , for $A^{q+} + H_2$ collisions (in units of 10^{-16} cm^2 and scaled as stated below). From below to above, lines correspond to collisions with different projectiles: H^+ (single plus double ionization), He^{2+} (data $\times 10$, single plus double ionization), Li^{3+} (data $\times 200$, single plus double ionization plus transfer ionization), Be^{4+} (data $\times 10$), B^{5+} (data $\times 5000$, single ionization).

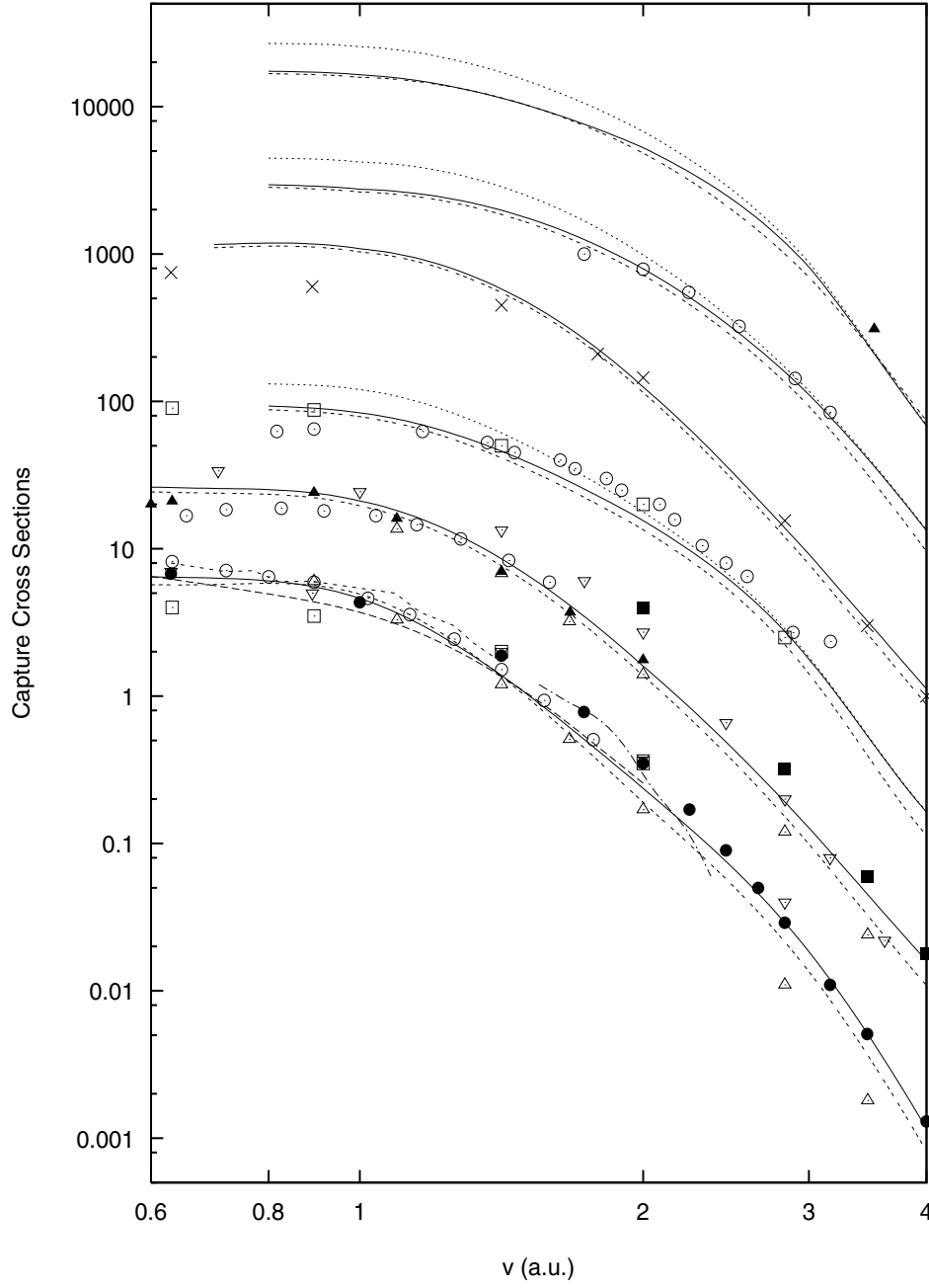


FIG. 13. SEC cross sections, as functions of the relative velocity v in a.u., for $A^{q+} + H_2$ collisions (in units of 10^{-16} cm^2 and scaled as stated below). From below to above, lines correspond to collisions with different projectiles: H^+ (single capture), He^{2+} (data $\times 2$, single capture), Li^{3+} (data $\times 5$, single capture plus transfer ionization), Be^{4+} (data $\times 50$, single capture), B^{5+} (data $\times 200$, single capture plus transfer ionization).